Forest Ecology and Management 432 (2019) 675–685

Contents lists available at ScienceDirect

Forest Ecology and Management

journal homepage: www.elsevier.com/locate/foreco

Discrepancy in tree transpiration of *Salix matsudana*, *Populus simonii* under distinct soil, topography conditions in an ecological rehabilitation area on the Northern Loess Plateau

Sheng Wang[a,b,c], Jun Fan[a,b,*], Jiamin Ge[b,c], Qiuming Wang[a], Wei Fu[a]

[a] State Key Laboratory of Soil Erosion and Dryland Farming on the Loess Plateau, Northwest A&F University, No. 3 Taicheng Road, Yangling 712100, Shaanxi, China
[b] Institute of Soil and Water Conservation, Chinese Academy of Sciences and Ministry of Water Resources, No. 26 Xinong Road, Yangling 712100, Shaanxi, China
[c] University of Chinese Academy of Sciences, No. 19 (A) Yuquan Road, Shijingshan District, Beijing 100049, China

ARTICLE INFO

Keywords:
Willow
Poplar
Soil texture
Infiltration
Soil drying
Fine root
Check-dam system

ABSTRACT

Complex naturally carved topography and large-scale artificial landforms significantly perturb hydrologic cycles and cause heterogeneity of water availability. Afforested trees exhibit distinct growth and survival strategies on distinct habitats on the Northern Loess Plateau in China. The objective of this study was to quantify tree transpiration discrepancies of two tree species aged > 30 years on different soil and topography conditions, and to explore the interactions with the atmosphere, hydrology, soil and topography, through long-term (up to seven years) observations of sap flow, meteorological factors and soil water contents (SWC). Results showed that mean whole-tree transpiration (T) of *Salix matsudana* and *Populus simonii* in the growing season were 46.7 and 175.2 kg d^{-1}, respectively, in a dam field, and were 5.6-fold and 4.2-fold the magnitude of that on a sloping field, respectively. Daily T was positively correlated ($P < 0.001$) with meteorological factors (i.e., reference evapotranspiration, ET_0; solar radiation, R_n; vapor- pressure deficit, VPD). Daytime ET_0 explained 37% of *S. matsudana* variation in T on the sloping field, up to 77% of the variation on a dam field, and 80% of the variation in T from *P. simonii* on both fields. The T of *S. matsudana* was significantly positively correlated with SWC from topsoil to 200 cm depth, and the correlation increased (partial R up to 0.55 at 200 cm depth) as depth increased on sloping field. However, no consistent correlations between T and shallow depth SWC existed on *S. matsudana* and *P. simonii* on dam fields and *P. simonii* on sloping field. Annual rainfall soil-water recharge depth reached up to 600 cm in wet years, but only 120 cm in dry years on sloping field with aeolian sandy soil, and was 200 cm even in wet years in dam field with loessial soil. Trees on the dam field absorbed water mainly from shallow groundwater. Tree fine roots gathered in the subsurface soil on the sloping field but not in the dam field indicated a root distribution adaption to precipitation patterns and water-use strategy. Soil water deficit formed in the 0–600 cm soil layer on the *S. matsudana* sloping field in normal and dry years, and soil water was replenished during wet years. Neither species is suitable for extensive revegetation implementation in this area due to their negative impacts on water resource sustainability.

1. Introduction

Water availability is a critical and restricting ecological factor in arid and semi-arid ecosystems (Chang et al., 2006). The Loess Plateau, situated in the northwest of China, is a unique critical zone with extensive and deep loess deposits (~640,000 km^2 in area, up to > 250 m in depth) featured as the most highly erodible soils on Earth (Jin et al., 2018). These soils are in an arid and semi-arid and continental monsoon climate (Jin et al., 2018). Soils in the area are characterized by severely eroded dense gullies and hills, fragmented landscapes, sparse vegetation and fragile ecosystems. Thus, starting in the 1950s, various government strategies such as revegetation, afforestation, construction of check dams, terracing and other eco-engineering practices have been implemented to remediate soil and water losses and restore ecological balance (Chen et al., 2015). For example, the Grain for Green project was launched in 1999 and is the largest active revegetation project in China or elsewhere (Deng et al., 2014; Zhang et al., 2018b). Consequently, following a large-scale land-use conversion of barren land or cropland into grassland, shrub land or forest, vegetation cover on the Loess Plateau has nearly doubled from 31.6% to 59.6% between 1999

* Corresponding author at: No. 26 Xinong Road, Yangling 712100, Shaanxi, China.
E-mail address: fanjun@ms.iswc.ac.cn (J. Fan).

https://doi.org/10.1016/j.foreco.2018.10.011
Received 23 August 2018; Received in revised form 30 September 2018; Accepted 3 October 2018

and 2013 (Chen et al., 2015). Both sediment discharge and runoff into the Yellow River have declined dramatically. However, continued excessive runoff and discharge decline have caused concerns over river safety and water supply in the lower reaches of the river (Chen et al., 2015; Yang and Lu, 2018). The negative impact of excessive or inappropriate revegetation and afforestation efforts, and the resultant soil drying has also been raised (Zhang et al., 2018b). The Loess Plateau is now threatened by a warming and drying due to climate changes, with more frequent climatic extremes likely to occur (Zhao et al., 2017). Thus, comprehensive knowledge on hydrological traits of rehabilitated vegetation and their interactions with the environment is essential to assess their eco-hydrological effects and guide future revegetation activities, and to work on a sustainability under changing climate.

Various studies have criticized the unbalanced revegetation-water relations on the Loess Plateau at both regional scales (Wang et al., 2018a, 2017; Zhang et al., 2018b) and from field observations (Jin et al., 2018; Zhang et al., 2018a). The introduction of exotic species, deep-rooted perennial vegetation and trees have been attributed to almost 80% of the current soil desiccation on the Loess Plateau (Chen et al., 2015; Shangguan, 2007). Poplar, willow, black locust and other tree species have been widely planted during afforestation, which contributed to a rapid expansion of tree cover on the Loess Plateau to 12% by 2014 (Wang et al., 2017). These trees usually absorb relatively more water from soil than grass and shrubs to satisfy their enormous canopy transpiration demands, and trees may extract shallow groundwater through deep root system; afforested trees likely worsen water-deficit related issues in water-limited regions (Tian et al., 2017). For instance, black locust, widely planted on the Loess Plateau, drew soil water down close to wilting point in the 0 to > 500 cm soil layers within < 5 years of planting in areas where the mean annual precipitation was < 600 mm (Liang et al., 2018).

By 2012, about 113,500 check dams were built on the Loess Plateau, creating 3200 km^2 of dam fields as small “alluvial plains” which have formed from sedimentation in front of check dams (Xu et al., 2004). Complex naturally carved topography (e.g., hills, slopes, gullies, plateaus, etc.) and large-scale artificial landforms (e.g., check-dam systems, terracing, etc.) have largely perturbed local hydrologic cycles and have caused uneven spatial distribution of water availability (Ambroise, 1995; Huang et al., 2013). Soil texture, closely related to soil water retention, is also an important factor influencing soil water availability (Dodd and Lauenroth, 1997; Hultine et al., 2006). Owing to previously mentioned reasons, afforested trees across the Loess Plateau have been found to differ in growth, survival status and morphology under distinct soil and topography conditions, even with exactly the same species and planting ages. “Stunted aged tree” depicts a common phenomenon on upland hills and slopes on the Northern Loess Plateau, in which a tree far less than its normal size struggles to survive under water scarcity and soil degradation after a long planting period (Aerts, 2013; Chen et al., 2008). However, the same tree species exhibited robust and even excessive growth in a gully and check-dam system, running a risk of consuming the limited water reservoirs (Peng et al., 2015).

So far, few studies have fully inspected the interactions between tree hydrological traits and complex topography as well as soil properties on afforestation. Majority of hydrology assessments of afforestation have been derived mainly from soil moisture measurements in the soil profile (Zhang et al., 2018a). However, water budgets do not accurately reflect tree hydrological traits with soil moisture measurements made to limited soil depths as tree roots can penetrate far deeper than practical monitoring depths into thick loess deposits. Quantifying of tree transpiration through sap flow methods facilitates *in situ*, automatic and continuous estimation of whole-tree water use (Cermak et al., 2004; Wang et al., 2018b). The thermal dissipation probe (TDP) method, also called the Granier method, is one of the most commonly used sap flow technique due to its simplicity, high degree of reliability as well as relatively low costs (Lu et al., 2004).

In this study, we measured sap flow of *Salix matsudana* and *Populus simonii* over up to successive seven growing seasons, from 2011 to 2017, which included dry, normal and wet years, in a sloping field site with an aeolian sandy soil and a dam field site with a loessial soil. We monitored meteorological conditions and soil-water conditions, and surveyed the root distribution and tree morphology. The objectives of this study were to (1) quantify the water use of two common afforested tree species in a water-wind erosion crisscross region on the Loess Plateau, (2) assess the effects of environmental factors on driving tree water use, including meteorological conditions and soil-water conditions, and (3) determine the interactions between tree hydrological traits and topography and soil textures.

2. Materials and methods

2.1. Site description

The study site was located in the Liudaogou Catchment (38.78° N, 110.35° E, and 1200 m a.s.l) in Shenmu City, Shaanxi Province, China. The catchment, west adjacent to Mu Us Desert, is within the Loess Plateau, China, referred to as the “water-wind erosion crisscross region”. It is characterized by many deep gullies and undulating slopes and hills. Fluvial and aeolian landforms are subject to periodic intense rainfall and winds that cause severe soil erosion (Fan et al., 2010). This area is in the continental monsoon climate zone and has a mean annual temperature of 8.4 °C. Mean annual precipitation (MAP) is 437 mm, of which 70% falls in intense rainstorms between July and September. Mean annual grass reference evapotranspiration (ET_0) from the FAO-56 Penman-Monteith equation (Allen et al., 2006) is approximately 1200 mm.

The dominant soil types in this area are a loessial soil and an aeolian sandy soil (Table 1). The loessial soil is developed directly from Quaternary loess parent material with elementary pedogenesis and is susceptible to water erosion. The aeolian sandy soil forms from coarse sandy soil deposits due to intense wind erosion and is distributed discontinuously on the undulating slopes and hills, implicating severe soil degradation and desertification having occurred. The aeolian sandy soil generally has coarse texture, poor cohesion, intense infiltrability, and low water retention. To harness the enormous soil and water losses and intercept water erosion sediments from loessial soil in hilly and gully areas, massive check dams had been built up behind the outlets of branch gullies, and dam fields have formed over several decades of loessial soil deposition within check dam system.

We selected two sites with distinct main soil and topography conditions. The first site is a level dam field site with loessial soil in a silted-up check dam system built about five decades prior to the experiment, and the second site a sloping field site with aeolian sandy soil. We

Table 1
Soil particle composition (%), soil texture, soil bulk density (BD, g cm^{-3}), field capacity (FC, cm^3 cm^{-3}) and wilting point (WP, cm^3 cm^{-3}) of two typical soils in the study plots. Classification of soil texture is based on the USDA system (Soil Science Division Staff, 2017).

Soil names	Soil particle contents (%)			Soil texture	BD (g cm^{-3})	FC (cm^3 cm^{-3})	WP (cm^3 cm^{-3})
	Sand (0.05–2 mm)	Silt (0.002–0.05 mm)	Clay (< 0.002 mm)				
Aeolian sandy soil	92.0	6.8	1.2	Sand	1.62	0.12	0.04
Loessial soil	52.5	35.8	11.7	Sandy loam	1.49	0.25	0.07

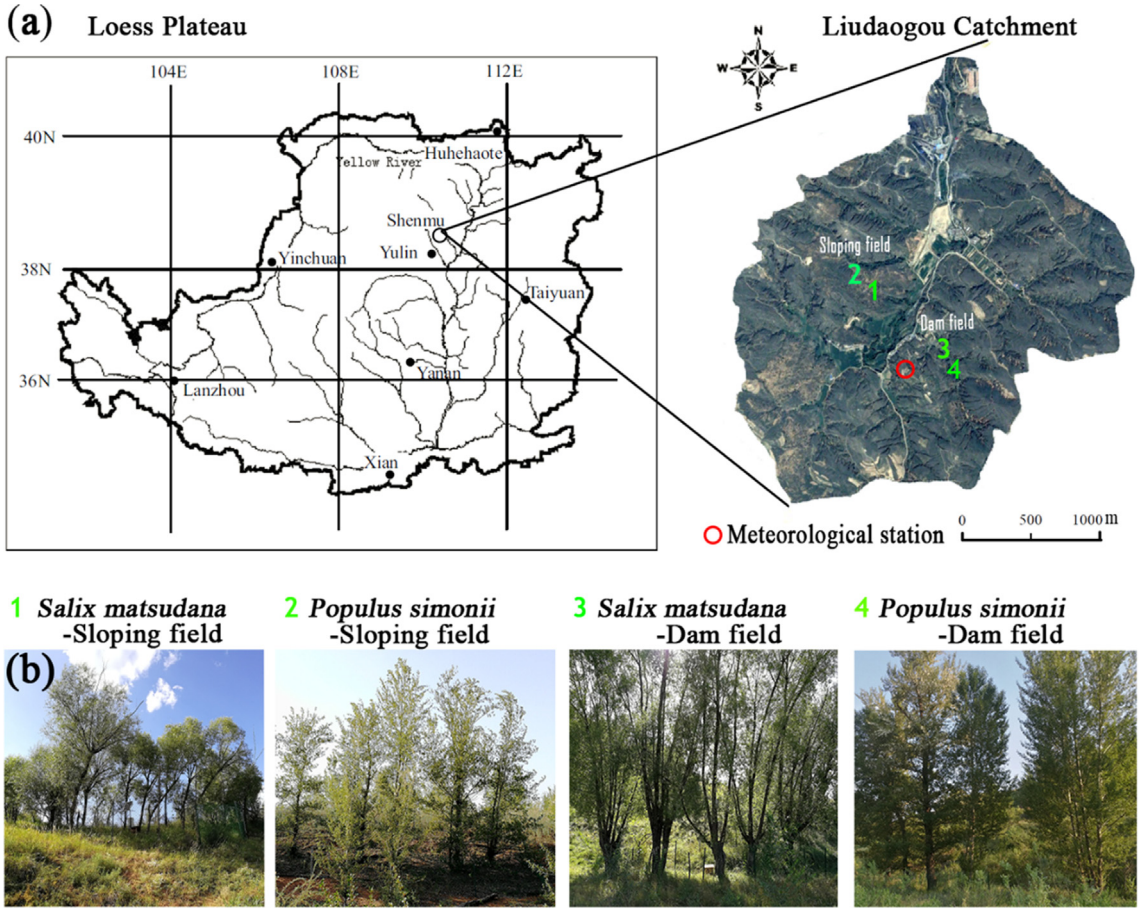

Fig. 1. (a) The location of the Liudaogou Catchment on the Loess Plateau, and positions of *S. matsudana* and *P. simonii* plots on the dam field and the sloping field sites, as well as meteorological station. (b) Photos of the corresponding four field plots.

Table 2
Basic information of study plots and sampled tree morphologic properties. DBH, diameter at breast height. Sapwood area was derived from sapwood depth investigated using a tree growth cone.

Study plots	Micro-topography	Species	Coordinates	Elevation (m)	Amount of sampled trees	Tree-tree spacing (m)	Height (m)	Mean canopy area (m2)	DBH (cm)	Sapwood area (cm^2)
Aeolian sandy soil, sloping field site										
No.1	Smooth sloping field	*Salix matsudana*	38.7946° N, 110.3642° E	1171	8	2.2 ± 1.3c*	4.5 ± 0.4d	5.6	12.3 ± 1.7d	47.8 ± 14.4d
No.2	Sloping groove	*Populus simonii*	38.7942° N, 110.3649° E	1175	5	2.9 ± 1.1b	10.7 ± 0.9c	9.1	18.7 ± 3.8c	218.3 ± 43.0c
Loessial soil, dam field site										
No.3	Level dam field	*Salix matsudana*	38.7979° N, 110.3596° E	1184	5	2.5 ± 0.7bc	17.9 ± 2.1b	23.2	35.5 ± 6.3b	242 ± 57.3b
No.4	Level dam field	*Populus simonii*	38.7983° N, 110.3588° E	1193	5	5.1 ± 1.9a	21.2 ± 3.3a	32.8	51.6 ± 7.9a	993.5 ± 122.7a
Meteorological station	Flat plateau	Short grass	38.7927° N, 110.3628° E	1210	–	–	–	–	–	–

* Note: Different lowercase letters beside numbers within a column denote significant difference among plots at 0.05 probability level with ANOVA and Tukey's HSD test.

selected plots with two local prevalent afforested tree species, *S. matsudana* and *P. simonii*, on each selected site. Both species have been widely planted beside roads and rives, around farmland and villages, in dam fields and main gullies, and on hilly sloping fields. A landscape of green veins with robust afforested trees occupies the gully and river system. Large areas of spare and stunted woodlands have also formed on the aeolian sandy soil covered sloping fields in this area. The distance between two plots in dam field site is 80 m. Unlike dam field site, two plots in sloping field sites had different micro-topographies. In one plot, *S. matsudana* stands on a smooth 5° gradient occupied the sloping field, while the other plot had *P. simonii* stands within a 30 m width groove between two undulated sloping ridges that were 75 m apart. Trees of both species were planted about four decades prior to the start of the experiment in dam field site, and were planted nearly three decades prior to the start of the experiment in the sloping field site. Basic information about the study plots and sampled tree morphologic properties is listed in Fig. 1 and Table 2.

2.2. Estimating transpiration through sap flow measurements

Sap flow rates were quantified by estimating sap-flux density using the TDP method. Sap flow measurement on the two *S. matsudana* plots were started in 2011 and ended in 2017. In two *P. simonii* plots, we conducted sap flow measurements in 2016 and 2017. Both species are deciduous, and start sprouting in April, and abscising leaves in late October. The sap flow measurements covered the growing season from May 1 to October 15.

Each TDP gauge consisted of a pair of temperature probes, one of which also housed a loop of resistance heating wire that acted as line source heater, and the other as a reference probe. When inserted into a tree trunk, the temperature and heater probe were inserted 5 cm above the reference probe, and were constantly heated by applying a small current through a resistance wire. Temperature difference (ΔT, °C) between the two probes was measured to derive sap-flux density (V_s, $cm^3\ cm^{-2}h^{-1}$) based on thermal dissipation through the moving sap, by an empirical equation (Granier, 1987)

$$Vs = 0.0119\left(\frac{\Delta T\,\max - \Delta T}{\Delta T}\right)^{1.231} \times 3600 \quad (1)$$

where ΔT_{max} denotes the maximum ΔT during a day or a longer period, which usually indicates a zero flow condition.

Specific TDP gauge configuration, construction and installation are detailed by Peng et al. (2015). Each sampled tree had two TDP gauges installed into trunk. Sap flow measurements had a 1-min scan rate and recorded the mean values at 30-min intervals. Sap flow rate (Fs, kg h^{-1}), is calculated as the product of V_s and cross-sectional sapwood area (A_s, cm^2), as

$$Fs = 0.001 \times Vs\ As \quad (2)$$

where A_s was derived from sapwood depth investigations using a tree growth cone. On the whole-tree level, we regarded transpiration (T) as approximately equivalent to sap flow rate through tree trunk.

2.3. Meteorology

A meteorological station located on a flat plateau in this catchment, as shown in Fig. 1 and described in Table 2, was 300 and 700 m away from the dam field site and the sloping field site, respectively. Air temperature, relative humidity, wind speed, solar radiation, soil heat flux and precipitation were measured at 5-s intervals and stored the mean or total values at 1-hour intervals. The ET_0 derived from FAO-56 Penman-Monteith equation (Allen, 2000; Allen et al., 2006) was used to scale atmosphere potential evapotranspiration, for daytime in hourly time steps, in unit mm h^{-1},

$$ET0 = \frac{0.408\Delta(Rn - G) + \gamma\frac{37}{T+237}u2\ VPD}{\Delta + \gamma\ (1 + 0.24u2)} \quad (3)$$

where Δ is slope of the saturation vapor pressure curve (kPa $°C^{-1}$), R_s is solar radiation (MJ $m^{-2}h^{-1}$), G is soil heat flux (MJ $m^{-2}h^{-1}$), γ is psychrometric constant (kPa $°C^{-1}$), T is air temperature at 2-m height (°C), u_2 is wind speed at 2-m height (m s^{-1}), and VPD denotes vapor-pressure deficit (kPa). For hourly or shorter periods,

$$VPD = 0.6108\,(1 - 0.01RH)\exp\left[\frac{17.27\ T}{T + 237.3}\right] \quad (4)$$

where RH denotes air relative humidity (%). Herein, hourly ET_0 is calculated using Ref-ET software (Version 4.1, https://www.uidaho.edu, University of Idaho, Kimberly, ID, USA).

2.4. Measurement of soil water contents

Two categories of soil water contents (SWC, $cm^3\ cm^{-3}$) were measured: (1) continuous monitoring in shallow soil depths, and (2) periodic monitoring in the soil profile. (1) The SWC dynamics at soil depths 10, 20, 50, 100 and 200 cm in each plot were continuously monitored by EC-5 sensors (Decagon Devices Inc., Pullman, WA, USA) at 1-h intervals. (2) Three representative locations, as duplications, were selected in each of two *S. matsudana* plots. Installation holes were drilled and access tubes were installed vertically into soil profile. SWC was measured through access tubes using a neutron probe (model CNC503B, Super Energy Nuclear Technology Ltd., Beijing, China) at 10-cm intervals to soil depth ≤100 cm and then at 20-cm intervals as soil depth was > 100 cm. These measurements were made once each month during growing season. On the sloping field plot, SWC from 0 to 600 cm soil depths was measured since 2013. In 2017, the depth of the SWC measurements increased to 1000 cm. On the dam field plot, the SWC was measured to depth 0–900 cm starting in 2016. Both the EC-5 sensors and the neutron probes were carefully calibrated by thermo-gravimetric method. Soil-water storage (SWS, mm) in specific soil layer is calculated as

$$SWS = \sum SWC_i d_i \quad (5)$$

where SWC_i denotes mean SWC of the ith sublayer ($cm^3\ cm^{-3}$), d_i is thickness of the ith sublayer (mm), and i is the number of sublayer.

2.5. Investigation of lateral root distribution

Both the *S. matsudana* and *P. simonii* have taproot systems. Their taproots are too deep to investigate. Their root fragments have been found at greater than 1000 cm depth in the soil profile in the dam field site. For practical reasons, only lateral root distribution in 0–400 cm soil layer was investigated using the soil core method. Each of the four plots selected six locations to collect undisturbed soil cores using a corer (10-cm diameter, 20-cm length). The soil cores were split at 20-cm intervals, and the roots were extracted and air-dried. Root samples were then scanned with an optical scanner and root images were processed using WinRHIZO software (Regents Instruments Inc., Quebec, Canada) for root measurements. Here, we used fine root (≤2 mm diameter) length density (RLD, km m^{-3}), which is the total fine root length per unit soil volume, to quantify the hydraulically-active lateral roots in the soil layer.

2.6. Data analysis

Mean daytime values of R_n, VPD and ET_0 were calculated, and daily T and SWC were obtained from 30-min and 1-hour interval data, respectively. Relationships between transpiration and meteorological factors, and soil-water conditions, were analyzed based on daily time scale data. This was done because sap flow may lag behind transpiration briefly, but transpiration only occurs when $R_s > 0$, which is the daytime (Chang et al., 2006). A linear regression analysis was performed using least squares to explore the relationship between T and meteorological factors. Partial correlation analysis was conducted to test the impact of soil-water conditions on T as ET_0 is controlled. To quantify T for the entire growing season, equations linearly relating daily T to mean daytime ET_0 were determined separately, based on observed data on each plot and each growing season, to interpolate the missing T data. Statistical analyses were performed with SPSS statistics ver. 18 (SPSS Inc., Chicago, USA).

3. Results

3.1. Precipitation characteristics

Precipitation (P) in the study area for more than a dozen of years – both prior to and during our experiment period – has been analyzed (Fig. 2). Intense variations of annual P occurred over 15 years, with a minimum of 280 mm in 2005 and a maximum of 704 mm in 2016. From 2003 to 2011, the area was constantly dry, with a mean P of 389 mm

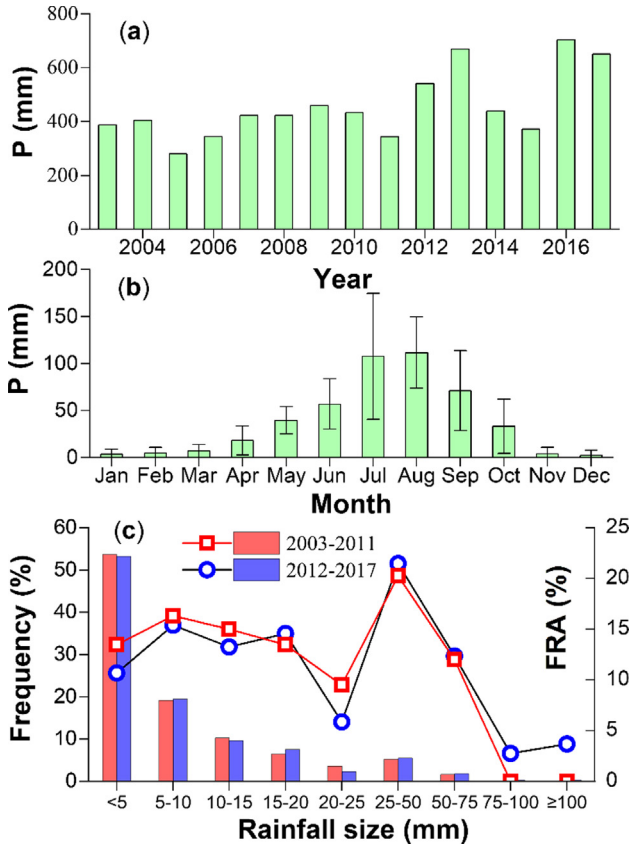

Fig. 2. Precipitation statistics from 2003 to 2017 in Liudaogou catchment. (a) Annual precipitation (*P*, mm), (b) monthly precipitation distribution, mean ± standard error, and (c) the frequency (%, bars) distribution and fraction of rainfall amount (FRA, %, lines + symbols) over different rainfall sizes from 2003 to 2011 and from 2012 to 2017, respectively.

per year, much lower than local MAP 437 mm. However, the area became wetter from 2012 onwards relative to the MAP. Mean *P* was 548 mm per year from 2012 to 2017, within which annual *P* was remarkably higher than MAP four out of the six years. For the other two years, *P* was almost equal to MAP in 2014, followed by a dry year with a *P* of 371 mm in 2015 (Fig. 2a).

Almost 80% of precipitation fell between May and September, corresponding to the growing season (Fig. 2b). Most rainfall events were small, with almost 55% of total events being < 5 mm and ~70% of total events with rainfall size < 10 mm. Other studies had indicated that an isolated rainfall of < 10 mm was ineffective to most forest ecosystems (Zhang et al., 2018a). The total sum of the small rainfall events < 10 mm accounted for up to ~30% of annual *P*. Only < 10% of total events were > 25 mm, however, they contributed ~40% of annual *P*. From 2012 to 2017, heavy rain occurred more frequently and rainfall intensity was higher compared to other years, and the inter-annual rainfall gap increased (Fig. 2c). In 2016, a single rainfall event equating to 127 mm within a day occurred on July 8, which is equivalent to nearly half of total precipitation of 2015. Evidently, local ecosystems are suffering an intensive regional changing climate with high climate uncertainty and frequent climate extremes.

3.2. Estimated whole-tree transpiration

On whole-tree level, mean *T* in the growing season of *S. matsudana* on the sloping field ranged from 5.8 to 10.7 kg d^{-1}, with an average of 8.3 kg d^{-1} over seven growing seasons. However, mean *T* of *S. matsudana* in dam field ranged from 42.3 to 51.4 kg d^{-1}, with an average of 46.7 kg d^{-1}, which is 5.6-fold of *T* on the sloping field. Mean *T* of *P. simonii* was 41.4 and 175.2 kg d^{-1} in growing seasons during 2016 and 2017, on sloping field and dam field, respectively. This indicated that whole-tree *T* of two species on the dam field was ~4-fold the magnitude of that on the sloping field. (Table 3).

3.3. Transpiration responses to meteorological factors

The relationships between daily whole-tree *T* and mean daytime ET_0, R_s and *VPD*, from May 15 to October 1, which was considered a constant tree canopy, were analyzed using the long-term field observation data (Fig. 3). Generally, *T* was extremely significant ($P < 0.001$) and positively linearly correlated with meteorological factors ET_0, R_s and *VPD* to both *S. matsudana* and *P. simonii* species, on distinct soil and topography conditions. This implied that meteorological conditions were the principal driving factors controlling *T* in the local niche. Scatterplots show daily *T* vs. meteorological factors of *S. matsudana*, which were distributed in a wider area in sloping field than in dam field. Univariate ET_0 explained 37% of variation in *T* of *S. matsudana* on the sloping field, however, ET_0 interpreted up to 77% of the variation in *T* on the dam field for the same tree species. Similar regular patterns also occurred to both R_s and *VPD*. We marked an area enclosed by two linear lines which contains 95% of scatterplots of *S. matsudana* over seven years, and approximately regarded the two lines as up-limit and down-limit of linear correlations between transpiration and meteorological factors (Fig. 3). The impact of restrictions of non-climate factors such as soil-water conditions, physiological stromal control, etc. was likely up to 76% on *S. matsudana* transpiration in sloping filed plot, but only 60% in dam field plot, without considering measurement errors. During the only two monitored years 2016 and 2017 for *P. simonii*, which were also the wet years, daytime ET_0 interpreted up to 80% of variations in daily *T*, both on sloping field and dam field plots.

Table 3
A summary of mean whole-tree transpiration (kg d^{-1}) and total field transpiration (mm) in growing season (from May 1 to October 15), and precipitation (*P*, mm) and grass reference evapotranspiration (ET_0, mm) in the growing season. The "–" symbol means the variable was not measured.

Year	Growing season		*S. matsudana*		*P. simonii*	
	P mm	ET_0 mm	Sloping field kg d^{-1}	Dam field kg d^{-1}	Sloping field kg d^{-1}	Dam field kg d^{-1}
2011	328.4	787.7	9	48.4	–	–
2012	440.1	733.6	7.6	42.3	–	–
2013	630.9	784.1	10.2	49.3	–	–
2014	342.2	740.1	6.6	44.3	–	–
2015	304.6	795.7	5.8	48.6	–	–
2016	564.4	712.7	7.9	42.3	39.4	169.41
2017	501	754.5	10.7	51.4	43.3	181.03
On average	444.5	758.3	8.3	46.7	41.4	175.2

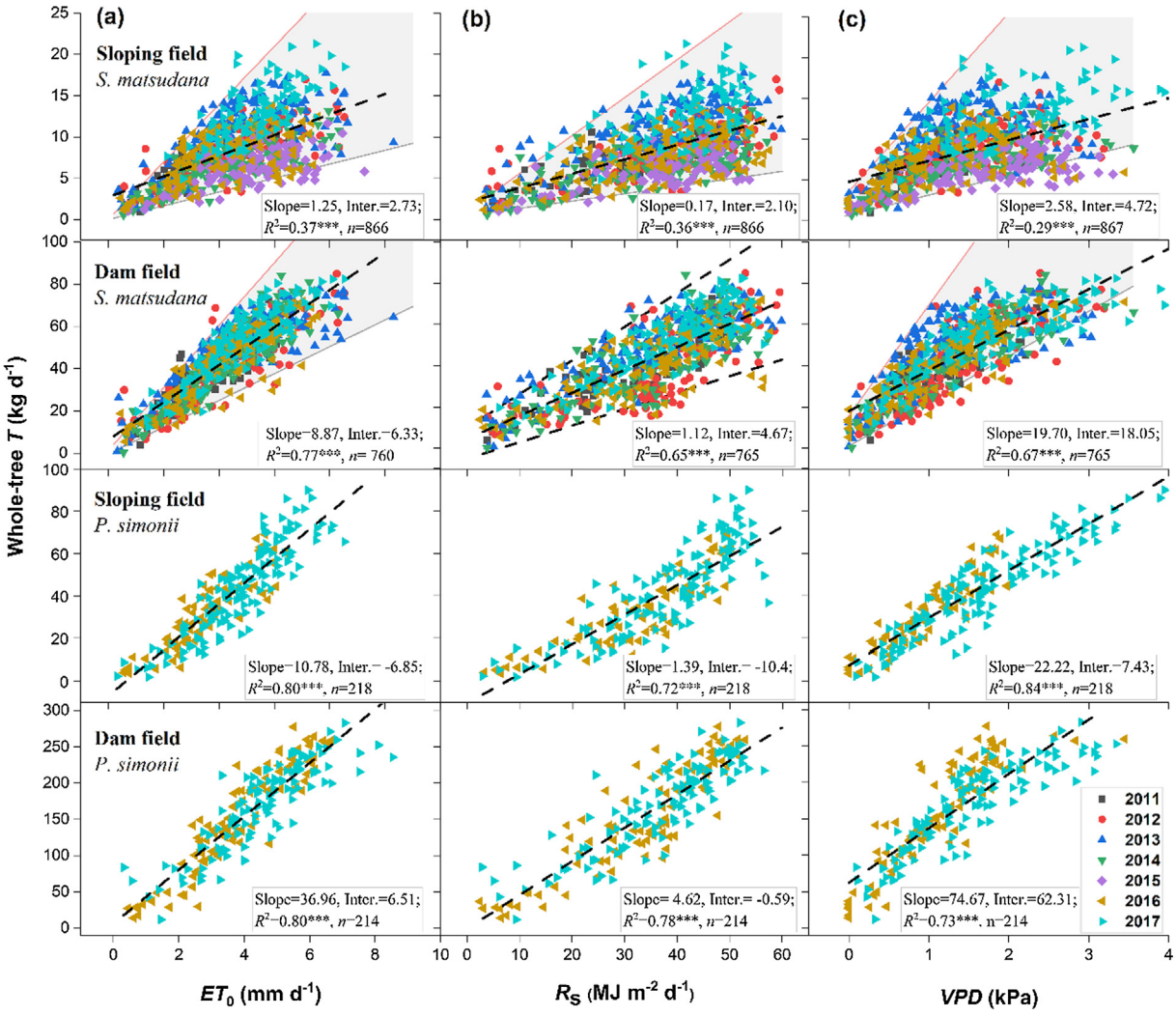

Fig. 3. Relationships between daily sap flow (kg d^{-1}) and mean daytime (a) grass reference evapotranspiration (ET_0, mm d^{-1}), (b) solar radiation (R_n, MJ m^{-2} d^{-1}), and (c) vapor-pressure deficit (*VPD*, kPa). The dashed line represents the linear regression line from the observed data in 2011–2017. Inter., intercept; n, number of data pairs; *** means $P < 0.001$.

3.4. Impact of soil-water conditions on transpiration

Discrepancy in soil-water conditions was observed over different soil and topography conditions. Contour plots in Fig. 4 showed the dynamics of SWC over soil depth and time. Mean SWC at 0–600 cm depth ranged from 0.04 to 0.09 cm^3 cm^{-3}, with an average of 0.06 cm^3 cm^{-3} in 2013–2017, in the sloping field plot with aeolian sandy soil. The soil profile was driest on June 2015, with a mean of SWC 0.043 cm^3 cm^{-3} at 0–600 cm depth. The soil was wettest with a mean of SWC 0.096 cm^3 cm^{-3}, on August 2017. The soil profile showed strong variations in SWC in both depth and time. In the dam field plot with loessial soil, mean SWC in the 0–1000 cm depth ranged from 0.11 to 0.16 cm^3 cm^{-3}, with an average of 0.14 cm^3 cm^{-3}, in 2016 and 2017. SWC showed more intense fluctuation in 0–250 cm depth than in at > 250 cm soil depth. At 250–400 cm soil depth, the SWC remained relatively stable and low, with a mean of 0.06 cm^3 cm^{-3}. At > 400 cm soil depth, SWC ascended gradually and reached up to 0.3 cm^3 cm^{-3} below a depth of ~800 cm. Abundant shallow groundwater occurred in the dam field, and the depth of groundwater level from ground surface undulated at ~7.5 m from our other observations.

On the sloping field with aeolian sandy soil, precipitation was almost the only soil water source through infiltration and redistribution to support plants. In the three wet years – 2013, 2016 and 2017 – rainfall quickly infiltrated and recharged to depth of up to or exceeding 600 cm at the start of the following growing season. In contrast, in a normal rainfall year, 2014, and a dry year, 2015, rainfall had recharged to a soil depth 120 and 160 cm by the end of the growing season, respectively, and soil water did not exceed 200 cm at the start of following growing season. On dam field with loessial soil, precipitation had more difficulty infiltrating through the heavy-textured soil layers. Even in wet years – 2013, 2016 and 2017 – the recharge depth was only 200 cm at the end of the growing season. In a dry year, 2015, the recharge depth was as shallow as 50 cm (Table 4).

Soil water was the primary plant water source. From partial correlation analysis (Fig. 5), daily *T* of *S. matsudana* in a sloping field were significantly positively correlated with SWC at soil depths of 10, 20, 50, 100 and 200 cm, and with soil water storage (SWS) in depths of 0–75, 75–300 and 0–300 cm under controlled ET_0 conditions. The degree of correlation between *T* and SWC became more intense at deeper soil depths, with a partial *R* value up to 0.6 at 200 cm depth. Results also indicated that SWS in 0–300 cm depth had the strongest correlation with *T*. This implied that *S. matsudana* absorbs soil water throughout from topsoil to deeper soil depths, and this had a significant impact on transpiration from the sloping field. In dam field, *T* of *S. matsudana* had a weak correlation with SWC in shallow depth, a strong correlation between *T* and ET_0, and therefore soil water at shallow depths made a small effect on *T*. Similarly, as to *P. simonii*, significant correlations between *T* and SWC existed at certain soil depths, but shallow soil

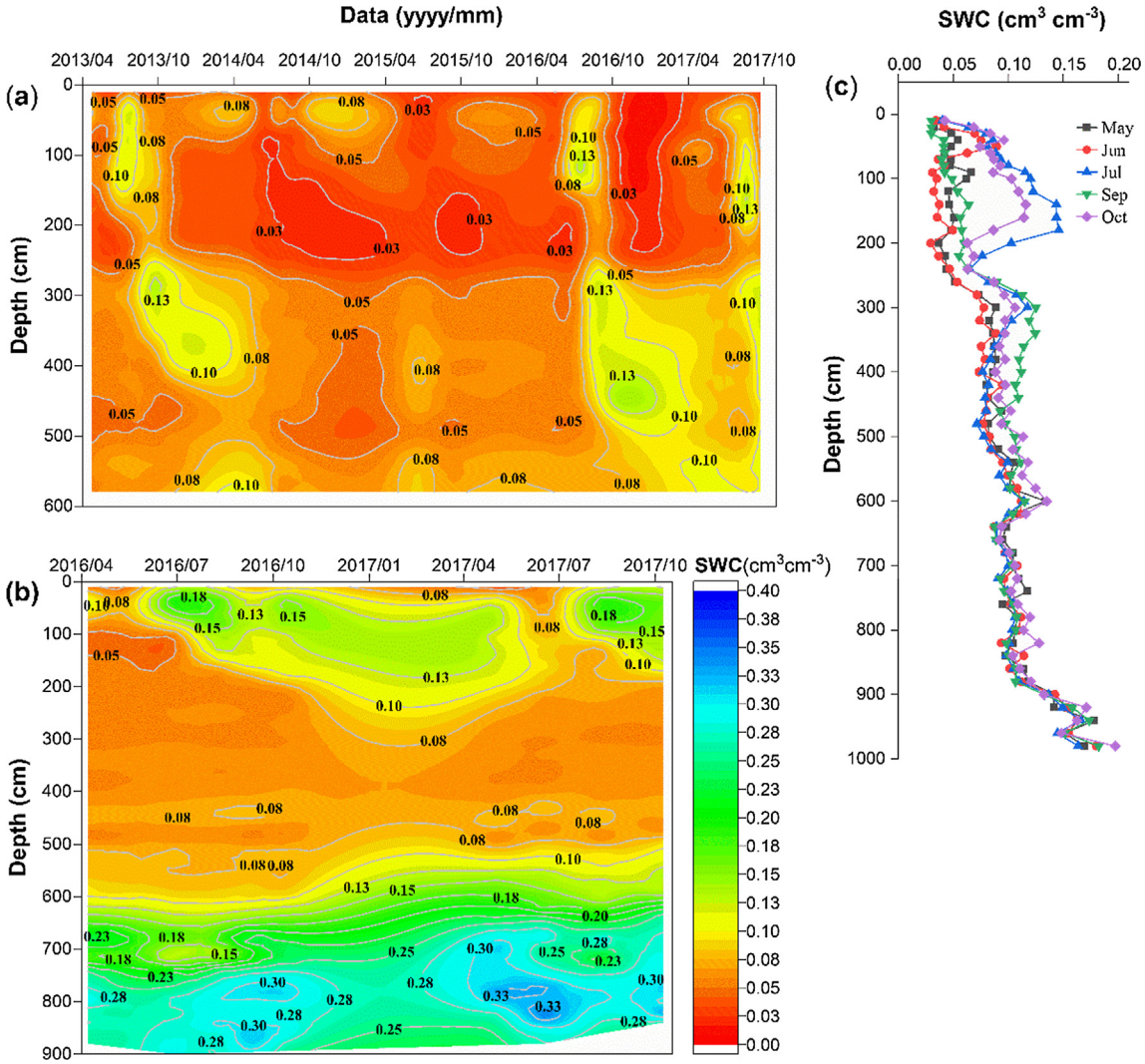

Fig. 4. Contour plots of soil water contents (SWC, $cm^3\ cm^{-3}$) over the soil profile depth (cm) and time series (Data, yyyy/mm), in (a) sloping field with aeolian sandy soil, and (b) dam field with loessial soil. Monitoring depth had been increased from 600 cm to 1000 cm on sloping field site in 2017, and (c) is the dynamics of SWC at 0–1000 cm soil depth on sloping field site in 2017.

Table 4
Soil water recharge depth (cm) from rainfall infiltration in the sloping field with aeolian sandy soil and the dam field with loessial soil.

Year	2013	2014	2015	2016	2017
Precipitation (mm)	669	439	371	704	651
Recharge depth (cm)					
Aeolian sandy soil, sloping field site					
End of growing season	420	120	160	600	600
Start of following growing season	> 600	180	200	> 600	> 600
Loessial soil, dam field site					
End of growing season	200	100	50	200	200
Start of following growing season	> 200	> 100	50	260	–

depth was not a principal soil water source in two wet years, both in the dam field and the sloping field.

3.5. Tree fine root distribution

The distribution of lateral fine roots with a diameter ≤2 mm in 0–400 cm soil layer in the four plots is presented in Fig. 6. The fine roots distribution in the soil profile were distinctly different between *S. matsudana* and *P. simonii*, and under distinct soil and topography conditions. On the sloping field site, fine *P. simonii* roots were nearly all (99%) distributed in 0–200 cm soil depth of the investigated 0–400 cm soil depth. The RLD reduced sharply as soil depth increased. Soil depth of 0–40 cm accommodated 67% of the fine roots; 52% of the fine roots were distributed in the 0–20 cm, and RLD were as high as 6860 km m^{-3} in this layer. Such high magnitude of fine roots in the subsurface will absorb high amounts of soil water after even small rainfall events during periods of drought to satisfy the enormous transpiration demands. However, *P. simonii* in dam field possessed 20% fewer of fine roots than that in sloping field, and ~5% of fine roots were distributed sporadically in depth 200–400 cm.

Overall, *S. matsudana* had less fine roots than *P. simonii* from 0 to 400 cm soil layer. Mean RLD of *S. matsudana* was 33% of that of the *P. simonii* in the sloping field, and 11% in the dam field. Similar to *P. simonii*, *S. matsudana* in sloping field also had a high RLD than in dam field; the RLD was 3.5-fold higher in the sloping field than in the dam field, and most of fine roots were distributed in the shallow soil depths of < 200 cm in sloping field.

4. Discussion

Revegetation strategies must consider water resource sustainability and ecosystem perseverance, especially in arid and semi-arid regions.

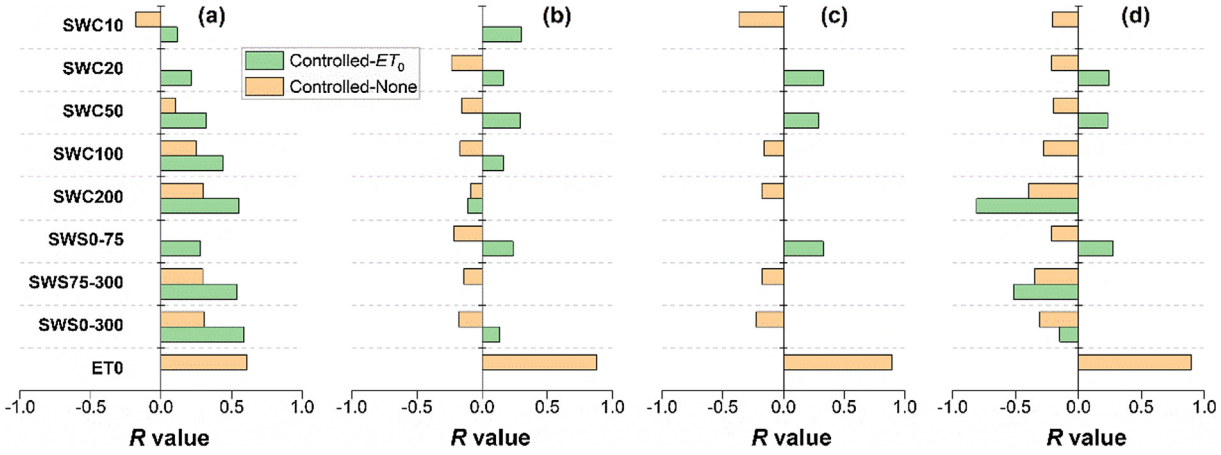

Fig. 5. Correlation coefficient (*R*) of partial correlation analysis between daily transpiration and soil-water conditions, including soil water contents (SWC, cm^3 cm^{-3}) at depth 10, 20, 50, 100 and 200 cm, and soil water storage (SWS, mm) in soil depths 0–75, 75–300 and 0–300 cm. (a) *S. matsudana* sloping field plot, (b) *S. matsudana* dam field plot, (c) *P. simonii* sloping field plot, and (d) *P. simonii* dam field plot. Green bars represent partial *R* under controlled grass reference evapotranspiration (ET_0, mm), and yellow bars denote zero-order partial correlation coefficient, i.e., no factors were controlled. (For interpretation of the references to colour in this figure legend, the reader is referred to the web version of this article.)

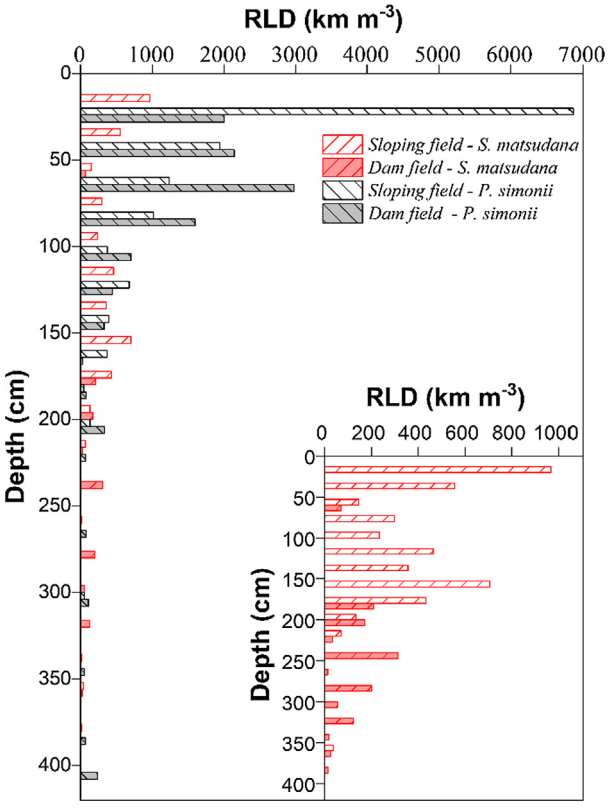

Fig. 6. Fine root length density (RLD, km m^{-3}) of *S. matsudana* and *P. simonii* plots in both sloping field and dam field sites. The roots were sampled at 20 cm depth-intervals using the soil core method. The small graph in lower right lists separately to show *S. matsudana* RLD in both sloping field and dam field sites distinctly.

Our study shows the differences in how two afforested tree species use water, and shows that tree transpiration was affected by tree morphology, hydrology, soil and topography. Large-scale human activities, such as the Grain for Green project, would generate a sustained impact on the regional hydroclimate and environment settings.

From our observations, soil desiccation occurred in the topsoil to a soil depth > 600 cm in both normal and dry years in aeolian sandy soil on a sloping field with *S. matsudana* planted three decades prior to the start of the experiment. During this time, SWC of 0.043 cm^3 cm^{-3} in 0–600 cm was measured in 2015, a dry year. We noticed that a SWS deficit of 85 mm to a soil depth 0–600 cm in 2014, a normal year. However, it was merely 3 mm in 2015, a dry year. The results implied that *S. matsudana* in drying soils possessed a root hydrologic functional plasticity to extend water uptake from deep soil when water stress occurred in the upper soil, which improved water use and supported the essential physiological water demand. Early studies also found that woody shrubs and trees progressively increase the depth of their water uptake when water becomes less available, and indicated a high degree of responsiveness of water uptake depth to changes in precipitation patterns (Asbjornsen et al., 2008). Tobella et al. (2017) found that *Vitellaria paradoxa*, an indigenous tree in semi-arid West Africa, obtains 90% of its water from depths of 10–50 cm in wet seasons, and shifts to deeper soil water sources during the dry seasons, obtaining 50% of its water from 30 to 600 cm depth and 30% from groundwater. Other studies have also shown that root depth span is significantly greater in dry conditions than in well-watered conditions in drying soils (Reader et al., 1993). North and Nobel (1998) indicated that this underlying root hydraulic functional plasticity implies the changes in root morphology, structure and anatomy; hydraulic conductivity architecture of roots gradually decreased under water-stress and resorted rapidly after rewetting. The underlying mechanism includes suberization, xylem maturation and mortality (North and Nobel, 1998), hydraulic transport patterns, osmotic adjustment (Blum, 2005), metabolism, carbon assimilation (Snyder and Williams, 2003) and activities of water channels (aquaporins) (Steudle, 2000), etc. triggered by water stress.

From lateral fine root distribution statistics, both *S. matsudana* and *P. simonii* on sloping field with aeolian sandy soil exhibited a considerably high intensity of fine roots in the subsurface soil which decreased as soil depth increased. This reflects an adaptation of their root distribution to adjust to local precipitation patterns. Locally, upland ecosystems with limited shallow groundwater availability are driven by a pulse of water availability from precipitation during the growing season. Here, precipitation falls most frequently as light rain, and the frequency decreased sharply as rainfall intensity became heavier (Fig. 2c). The depth of water replenishment is strongly related to rainfall intensity, and subsurface depths could profit from frequent soil rewetting which would provide quite regular and considerable water availability. However, deeper soil layers are recharged less often. The gathering of fine roots in the subsurface benefits trees by obtaining water early and much as possible. However, they must compete against understory herbaceous and shrub plants for water (Ogle and Reynolds,

2004), resulting in a degradation of biodiversity and plant communities (Asbjornsen et al., 2008). Thanks to high rates of water permeability in the aeolian sandy soil, water replenishment was quick and deep which supported the existence of high water-consumption trees in fields with limited groundwater availability. This suggests that most afforested trees survive on sandy soil field rather than on loessial soil field with poor water permeability. The occurrence of heavy rains, especially rainstorms, results in a large portion of rainfall penetrating quickly through coarse-textured soil and providing abundant water availability and reservoirs to deep depths, even recharging groundwater. This benefits the soil water environment, and helps the growth and survival of trees, however, such rainfall extremes may also cause soil and water losses, as well as geologic hazards. Otherwise, continuous and perennial dry growing seasons would force trees to exhaust water reservoirs from deep soils and endanger trees for subsisting.

The effects of topography on tree transpiration is largely associated with the redistribution of water availability. The influx of subsurface interflow is intercepted and reservoirs as abundant shallow groundwater within the check-dam system (Huang et al., 2013; Yasuda et al., 2013). Soil moisture enrichment also occurs in gullies and micro-topographies of water converge in this area and form a distinctively moist soil-water environment and vegetational landscape compared to the common situation (Yasuda et al., 2010). From our observations, the whole-tree *T* of both tree species in the dam field site was 4.2- to 5.6-fold of that on the sloping field site, mainly due to the ample water supply from shallow groundwater. Even on sloping plot site, *T* of *P. simonii* in the sloping groove was weakly correlated with soil-water conditions but strongly correlated with ET_0, and were distinctively different with *S. matsudana* on the sloping field. This implies that the groove had far better soil-water conditions at deeper soil depths than the smooth sloping field. Apart from soil and topography conditions, the species of plants which have distinct constitutive physiological and physical traits largely affects the magnitude and pattern of water use. The whole-tree *T* of *P. simonii* was ~4-fold as that of *S. matsudana* with the same soil and topography, thus selecting proper species is crucial for revegetation projects. Neither *S. matsudana* nor *P. simonii* are suitable for extensive implementation in this area. Unlike in sloping field, the growth and survival of them in the dam field is seldom threatened by water scarcity. However, we estimated that *S. matsudana* and *P. simonii* absorbed an average of ~8000 and 28,000 kg water, respectively, per single tree in a growing season in the dam field. Such magnitude of water consumption will negatively impact shallow groundwater resources, which are needed to sustain regional hydrological balance. Related studies in this area are still rare, and more research is needed. The dam field was the only remaining high-productivity land for local agricultural production, on which extensive afforestation will jeopardize food safety and irrigation water supply.

Water use and hydraulic traits of afforested plants interacted with hydrology, topography, soil texture, etc. However, their relative importance varied. With the *S. matsudana* on the sloping field, the mean *T* during an entire growing season had an apparent increase with *P*, but no such tendency was observed in the dam field. Discordantly, with the *S. matsudana* on the dam field, the mean *T* during an entire growing season had a significant increasing trend with ET_0, however, no such trend was observed in the sloping field (Fig. 7). Tree density, an important factor but not fully discussed in this study, significantly impacts regional hydrology and energy balance, and the development of ecological rehabilitation (Giambelluca et al., 2009). In the study area, afforested tree stands or patches often occupy different tree densities and canopy structures. Thus we carry on analyses mainly based on whole-tree level rather than stand level, due to the incomparability of tree density and canopy structure in different plots. We noted that, as local climate had become much wetter overall during our experiments than prior to, so physiological and morphological evolution of the tree community was inevitable and occurred gradually to adjust to the changing climate, and as a result, alternative stable states then will

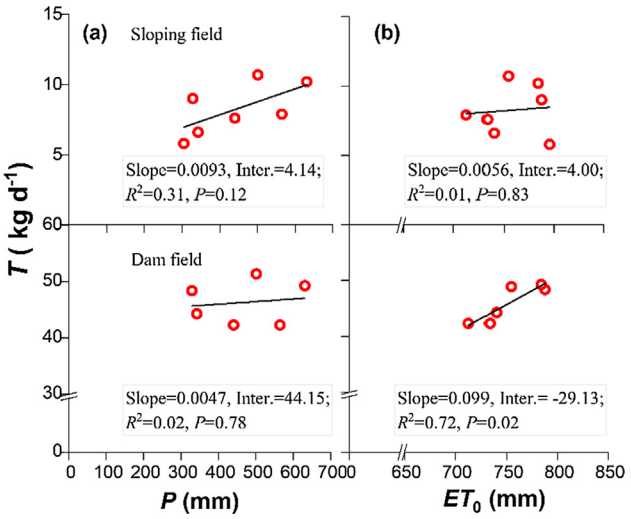

Fig. 7. The relationship between mean whole-tree transpiration (*T*, mm d^{-1}) of *S. matsudana* and precipitation (*P*, mm; a) and grass reference evapotranspiration (ET_0, mm; b) in growing season (from May 1 to October 15) over years from 2011 to 2017, in both sloping field and dam field sites.

establish (Robinson et al., 2016). Better knowledge of these interactions will facilitate better water use prediction, ecological effect assessments and future rehabilitation strategy adjustments. Future studies are still required concerning the underlying plant hydrologic physiological mechanisms, the hydrologic linkage between subsurface soil and deep soil by rooting systems, and hydrological impacts of planting structures, for instance, tree density.

Besides afforestation, widespread native grassland, deep-rooted forage land and shrub land have also formed on the prior cropland or barren land in this region, following the implementation of revegetation projects. Fan et al. (2016) reported that both forage (alfalfa, i.e. *Medicago sativa*) land and shrub (*Caragana korshinskii*) land with a typical loessial soil depleted soil water to below 600 cm soil depth, however, local rainfall could only recharge soil water to 120 cm soil depth. Forage steps towards retrogression after severe soil water deficit occurs in several years of planting. The revegetated native grassland was observed a balanced soil water depletion and recharge depths only to a maximum of 300 cm (Fan et al., 2016), and proved to significantly decrease soil erodibility, reduce hillslope runoff (Wang et al., 2013), and enrich ecosystem carbon sequestration (Wang et al., 2016). It implies that future revegetation strategies in this region should consider natural grass restoration as major approach towards sustainable soil and water resources use and ecosystem perseverance. However, when trees and shrubs still need to be considered in revegetation practices for certain purposes, the concept of "soil water-carrying capacity for vegetation (SWCCV)" – defined as "the maximum biomass of a given type of vegetation, under specific climatic conditions, soil texture, and management regime, that a given arid or semi-arid area can sustain without diminishing the capacity of soil water to support future generations" (Xia and Shao, 2009; Liu and Shao, 2015; She et al., 2014; Fu et al., 2012) – should be considered in designing the allowable planting density to avoid aggravating soil-water environments. But works on SWCCV are still elementary in this region, further work is still needed to guide scientific revegetation design.

5. Conclusions

The present study quantifies and compares tree transpiration discrepancy of two species *S. matsudana* and *P. simonii* commonly used in afforestation under distinct soil and topography conditions on the Northern Loess Plateau. It concludes that, whole-tree *T* of *P. simonii* is ~4-fold that of *S. matsudana*; they growing in the dam field plots

consume soil water 4.2- to 5.6-fold the magnitude of that in the upland sloping field site. Meteorological conditions were the principal factors driving tree transpiration, but the extent of their impacts distinctly differs in different niches with dissimilar soil-water conditions. Trees have different water use strategies, they use shallow soil water as an important water source besides deep soil water in the upland sloping field site; discordantly, they absorb shallow groundwater as principle water source in the dam filed site. Soil and topography conditions impact tree water use mainly through redistributing water availability. From lateral root distribution analysis, we found a root distribution adaption to local precipitation patterns, soil-water conditions and tree water-use strategies.

It is important to take scientific revegetation strategies with balanced plant-water relations in arid and semi-arid regions. Neither *S. matsudana* nor *P. simonii* is suitable for extensive revegetation implementation in this area due to their negative impacts on water resource sustainability. In future revegetation practices, we recommend natural grass restoration as major approach towards sustainable soil and water resources use and ecosystem perseverance. We should consider “soil water-carrying capacity for vegetation” and carefully control the planting density within the allowable values, if high water-consumption trees and shrubs need to be used in revegetation practices.

Acknowledgements

We acknowledge funding by the National Natural Science Foundation of China (No. 41571224) and Western Youth Scholar of the Chinese Academy of Sciences (XAB2015A03). We also thank the editors and the anonymous reviews for their diligent work and pertinent, valuable suggestions for substantially improving this article.

Appendix A. Supplementary material

Supplementary data to this article can be found online at https://doi.org/10.1016/j.foreco.2018.10.011.

References

Aerts, R., 2013. Old trees: extraction, conservation can coexist. 904 904. Science 339 (6122). https://www.doi.org/10.1126/science.339.6122.904-a.
Allen, R.G., 2000. Using the FAO-56 dual crop coefficient method over an irrigated region as part of an evapotranspiration intercomparison study. J. Hydrol. 229 (1–2), 27–41. https://doi.org/10.1016/S0022-1694(99)00194-8.
Allen, R.G., et al., 2006. A recommendation on standardized surface resistance for hourly calculation of reference ETo by the FAO56 Penman-Monteith method. Agr. Water Manage. 81 (1–2), 1–22. https://doi.org/10.1016/j.agwat.2005.03.007.
Ambroise, B., 1995. Topography and the water cycle in a temperate middle mountain environment: the need for interdisciplinary experiments. Agr. Forest Meteorol. 73 (3–4), 217–235. https://doi.org/10.1016/0168-1923(94)05076-I.
Asbjornsen, H., et al., 2008. Seasonal patterns in depth of water uptake under contrasting annual and perennial systems in the Corn Belt Region of the Midwestern US. Plant Soil 308 (1–2), 69–92. https://doi.org/10.1007/s11104-008-9607-3.
Blum, A., 2005. Drought resistance, water-use efficiency, and yield potential – are they compatible, dissonant, or mutually exclusive? Aust. J. Agr. Res. 56 (1), 1159–1168. https://doi.org/10.1071/AR05069.
Cermak, J., et al., 2004. Sap flow measurements with some thermodynamic methods, flow integration within trees and scaling up from sample trees to entire forest stands. Trees-Struct. Funct. 18 (5), 529–546. https://doi.org/10.1007/s00468-004-0339-6.
Chang, X.X., et al., 2006. Sap flow and tree conductance of shelter-belt in and region of China. Agr. Forest Meteorol. 138, 132–141. https://doi.org/10.1016/j.agrformet.2006.04.003.
Chen, H.S., et al., 2008. Soil desiccation in the Loess Plateau of China. Geoderma 143 (1–2), 91–100. https://doi.org/10.1016/j.geoderma.2007.10.013.
Chen, Y.P., et al., 2015. Balancing green and grain trade. Nat. Geosci. 8, 739–741. https://www.nature.com/articles/ngeo2544.
Deng, L., et al., 2014. Land-use conversion and changing soil carbon stocks in China's 'Grain-for-Green' Program: a synthesis. Global Change Biol. 20 (11), 3544–3556. https://doi.org/10.1111/gcb.12508.
Dodd, M.B., Lauenroth, W.K., 1997. The influence of soil texture on the soil water dynamics and vegetation structure of a shortgrass steppe ecosystem. Plant Ecol. 133 (1), 13–28. https://doi.org/10.1023/A:1009759421640.
Fan, J., et al., 2010. Toward sustainable soil and water resources use in China's highly erodible semi-arid loess plateau. Geoderma 155 (1–2), 93–100. https://doi.org/10.1016/j.geoderma.2009.11.027.
Fan, J., et al., 2016. Soil water depletion and recharge under different land cover in China’s Loess Plateau. Ecohydrology 9, 396–406. https://doi.org/10.1002/eco.1642.
Fu, W., et al., 2012. Optimization of plant coverage in relation to water balance in the Loess Plateau of China. Geoderma 173–174, 134–144. https://doi.org/10.1016/j.geoderma.2011.12.016.
Giambelluca, T.W., et al., 2009. Evapotranspiration and energy balance of Brazilian savannas with contrasting tree density. Agr. Forest Meteorol. 149 (8), 1365–1376. https://doi.org/10.1016/j.agrformet.2009.03.006.
Granier, A., 1987. Evaluation of transpiration in a douglas-fir stand by means of sap flow measurements. Tree Physiol. 3 (4), 309–319. https://doi.org/10.1093/treephys/3.4.309.
Huang, J.B., et al., 2013. Effects of the check dam system on water redistribution in the Chinese Loess Plateau. J. Hydrol. Eng. 18 (8), 929–940. https://doi.org/10.1061/(ASCE)HE.1943-5584.0000689.
Hultine, K.R., et al., 2006. Influence of soil texture on hydraulic properties and water relations of a dominant warm-desert phreatophyte. Tree Physiol. 26 (3), 313–323. https://doi.org/10.1093/treephys/26.3.313.
Jin, Z., et al., 2018. Soil moisture response to rainfall on the Chinese Loess Plateau after a long-term vegetation rehabilitation. Hydrol. Process. 32 (12), 1738–1754. https://doi.org/10.1002/hyp.13143.
Liang, H.B., et al., 2018. Soil moisture decline following the plantation of *Robinia pseudoacacia* forests: evidence from the Loess Plateau. Forest Ecol. Manage. 412, 62–69. https://doi.org/10.1016/j.foreco.2018.01.041.
Liu, B.X., Shao, M.A., 2015. Modeling soil–water dynamics and soil–water carrying capacity for vegetation on the Loess Plateau. China. Agr. Water Manage. 159, 176–184. https://doi.org/10.1016/j.agwat.2015.06.019.
Lu, P., et al., 2004. Granier's thermal dissipation probe (TDP) method for measuring sap flow in trees: theory and practice. Acta Bot. Sinica-English Ed. 46 (6), 631–646. https://www.ishs.org/sites/default/files/documents/lu2004.pdf.
North, G.B., Nobel, P.S., 1998. Water uptake and structural plasticity along roots of a desert succulent during prolonged drought. Plant Cell Environ. 21 (7), 705–713. https://doi.org/10.1046/j.1365-3040.1998.00317.x.
Ogle, K., Reynolds, J.F., 2004. Plant responses to precipitation in desert ecosystems: integrating functional types, pulses, thresholds, and delays. Oecologia 141 (2), 282–294. https://doi.org/10.1007/s00442-004-1507-5.
Peng, X.P., et al., 2015. Discrepancy of sap flow in Salix matsudana grown under different soil textures in the water-wind erosion crisscross region on the Loess Plateau. Plant Soil 390 (1–2), 383–399. https://doi.org/10.1007/s11104-014-2333-0.
Reader, R.J., et al., 1993. A comparative-study of plasticity in seedling rooting depth in drying soil. J. Ecol. 81 (3), 543–550. https://www.jstor.org/stable/2261532.
Robinson, D.A., et al., 2016. Experimental evidence for drought induced alternative stable states of soil moisture. Sci. Rep.-UK 6. https://doi.org/20018.10.1038/srep20018(2016).
Shangguan, Z.P., 2007. Soil desiccation occurrence an its impact on forest vegetation in the Loess Plateau of China. Int. J. Sust. Dev. World Ecol. 14 (3), 299–306. https://doi.org/10.1080/13504500709469730.
She, D.L., et al., 2014. Modeling effects of land use and vegetation density on soil water dynamics: implications on water resource management. Water Resour. Manage. 28, 2063–2076. https://doi.org/10.1007/s11269-014-0599-x.
Snyder, K.A., Williams, D.G., 2003. Defoliation alters water uptake by deep and shallow roots of Prosopis velutina (Velvet Mesquite). Funct. Ecol. 17 (3), 363–374. https://doi.org/10.1046/j.1365-2435.2003.00739.x.
Soil Science Division Staff, 2017. Soil survey manual. In: Ditzler, C., Scheffe, K., Monger, H.C. (Eds.), USDA Handbook 18, fourth ed. Government Printing Office, Washington, D.C.
Steudle, E., 2000. Water uptake by plant roots: an integration of views. Plant Soil 226 (1), 45–56. https://doi.org/10.1023/A:1026439226716.
Tian, F., et al., 2017. Effects of revegetation on soil moisture under different precipitation gradients in the Loess Plateau, China. Hydrol. Res. 48 (5), 1378–1390. https://doi.org/10.2166/nh.2016.022.
Tobella, A.B., et al., 2017. Strategies trees use to overcome seasonal water limitation in an agroforestry system in semiarid West Africa. Ecohydrology 10 (3), e1808. https://doi.org/10.1002/eco.1808.
Wang, B., et al., 2013. Effect of natural restoration time of abandoned farmland on soil detachment by overland flow in the Loess Plateau of China. Earth Surf. Process. Landforms 38, 1725–1734. https://doi.org/10.1002/esp.3459.
Wang, F.T., et al., 2018a. Is afforestation-induced land use change the main contributor to vegetation dynamics in the semiarid region of North China? Ecol. Indic. 88, 282–291. https://doi.org/10.1016/j.ecolind.2017.12.061.
Wang, K.B., et al., 2016. Dynamics of ecosystem carbon stocks during vegetation restoration on the Loess Plateau of China. J. Arid Land 8 (2), 207–220. https://doi.org/10.1007/s40333-015-0091-3.
Wang, S., et al., 2018b. New design of external heat-ratio method for measuring low and reverse rates of sap flow in thin stems. Forest Ecol. Manage. 419–420, 10–16. https://doi.org/10.1016/j.foreco.2018.03.020.
Wang, Y.H., et al., 2017. The spatiotemporal variation of tree cover in the Loess plateau of china after the 'grain for green' project. Sustainability 9 (5), 739. https://doi.org/10.3390/su9050739.
Xia, Y.Q., Shao, M.A., 2009. Evaluation of soil water-carrying capacity for vegetation: the concept and the model. Acta Agr. Scand. B.-S. P. 59, 342–348. https://doi.org/10.1080/09064710802203537.
Xu, X.Z., et al., 2004. Development of check-dam systems in gullies on the Loess Plateau. China. Environ. Sci. Policy 7 (2), 79–86. https://doi.org/10.1016/j.envsci.2003.12.002.
Yang, K.J., Lu, C.H., 2018. Evaluation of land-use change effects on runoff and soil erosion of a hilly basin the Yanhe River in the Chinese Loess Plateau. Land Degrad. Dev.

29 (4), 1211–1221. https://doi.org/10.1002/ldr.2873.
Yasuda, H., et al., 2013. The impact of plant water uptake and recharge on groundwater level at a site in the Loess Plateau of China. Hydrol. Res. 44 (1), 106–116. https://doi.org/10.2166/nh.2012.241.
Yasuda, N., et al., 2010. Performance evaluation of a tailings pond seepage collection system. Can. Geotech. J. 47 (12), 1305–1315. https://doi.org/10.1139/T10-029.
Zhang, Q.Y., et al., 2018a. Revegetation with artificial plants improves topsoil hydrological properties but intensifies deep-soil drying in northern Loess Plateau. China. J. Arid Land 10 (3), 335–346. https://doi.org/10.1007/s40333-018-0007-0.
Zhang, S.L., et al., 2018b. Excessive afforestation and soil drying on China's Loess. Plateau. J. of Geophys. Res.-Biogeo. 123 (3), 923–935. https://doi.org/10.1002/2017JG004038.
Zhao, X.K., et al., 2017. Climatic and drought characteristics in the loess hilly-gully region of China from 1957 to 2014. Plos One 12 (6), e0178701. https://doi.org/10.1371/journal.pone.0178701.